Ground motion optimised orbit feedback design for the future linear collider

J. Pfingstner[a,b], J. Snuverink[a,c], D. Schulte[a]

[a] *CERN, Geneva 23, CH-1211, Switzerland*
[b] *Graz University of Technology, Rechbauerstr. 12, 8010 Graz, Austria*
[c] *John Adams Institute at Royal Holloway, University of London, Surrey, UK*

Abstract

The future linear collider has strong stability requirements on the position of the beam along the accelerator and at the interaction point (IP). The beam position will be sensitive to dynamic imperfections in particular ground motion. A number of mitigation techniques have been proposed to be deployed in parallel: active and passive quadrupole stabilisation and positioning as well as orbit and IP feedback. This paper presents a novel design of the orbit controller in the main linac and beam delivery system. One global feedback controller is proposed based on an SVD-controller (Singular Value Decomposition) that decouples the large multi-input multi-output system into many independent single-input single-output systems. A semi-automatic procedure is proposed for the controller design of the independent systems by exploiting numerical models of ground motion and measurement noise to minimise a target parameter, e.g. luminosity loss. The novel design for the orbit controller is studied for the case of the Compact Linear Collider (CLIC) in integrated simulations, which include all proposed mitigation methods. The impact of the ground motion on the luminosity performance is examined in detail. It is shown that with the proposed orbit controller the tight luminosity budget for ground motion effects is fulfilled and accordingly, an essential feasibility issue of CLIC has been addressed. The orbit controller design is robust and allows for a relaxed BPM resolution, while still maintaining a strong ground motion suppression performance compared to traditional methods. We believe that the described method could easily be

Email address: `juergen.pfingstner@cern.ch, +41767075119` (J. Pfingstner)

Preprint submitted to Elsevier *November 5, 2012*

applied to other accelerators and light sources.

Keywords: orbit feedback system, ground motion, SVD decoupling

1. Introduction

The future linear collider [1, 2] requires beam sizes at the interaction point in the nanometre range to achieve its nominal luminosity. These requirements make the luminosity performance sensitive to ground motion. Ground motion misaligns the accelerator components over time, which excites beam oscillations. These beam oscillations degrade the average luminosity via generated beam-beam offset and emittance increase due to filamentation [3]. The ground motion problem is considered to be a severe feasibility issue for the design of the future linear collider.

Several mitigation methods have been put in place to cope with the ground motion issue. While static component misalignments are cured with the help of beam-based alignment [4] and tuning methods [5], the effect of dynamic misalignments is reduced with mechanical stabilisation systems [6] and beam-based feedback controllers. In this paper, we present a novel design strategy for the orbit controller for dynamic alignment in the main linac and the beam delivery system of the future linear collider.

Significant contributions to the topic of orbit feedback systems for linear accelerators have already been achieved, e.g. for the Stanford Linear Collider (SLC) at SLAC [7] and the Next Linear Collider (NLC) summarised in [8]. These feedback systems are based on local correction sections that are exchanging information among each other in order to avoid overcorrection. This local nature was introduced to cope with model errors and measurement noise. However, in [8] it is mentioned that better performance was achieved by moving from many local feedback systems to fewer more global ones. As a result of this observation, we present in this work a global feedback strategy similar to the ones use in circular colliders [9, 10]. The design is especially optimised to cope with the higher sensitivity of the global feedback to model errors and measurement noise.

After the introduction of the necessary models of the accelerator, ground motion and ground motion effects on the beam oscillations in section 2, the proposed orbit control algorithm is presented in section 3. It is based on the decoupling of the inputs (correctors) and outputs (measurements of the beam position monitors (BPMs)) of the accelerator system with the help of the *singular value decomposition* (SVD), which is a well known approach for orbit controllers [9, 10]. The innovation of the design in this paper is a method to design each individual controller for the decoupled accelerator systems. A semi-automatic procedure is proposed to choose open controller parameters, such that a given target function (average beam orbit, emittance or luminosity) is minimised with respect to ground motion excitation and measurement noise. The designer still has the freedom to incorporate important system knowledge in the design procedure. Since each controller does not have to be hand-tuned, the design time is significantly reduced.

Also other orbit controller designs aim to minimise a given target function with respect to the mentioned excitation signals, but do this only in a qualitative way. The proposed method, on the other hand, uses explicit models of the ground motion, the measurement noise and the influence of these signals on the target function. In this way, the presented design method can incorporate the rich ground motion knowledge [11, 12] in a quantitative manner. This model-based approach improves the efficiency of the ground motion suppression. Additionally, the found controllers are robust with respect to measurement noise, since this imperfection has been explicitly included in the design procedure.

In section 4 the proposed design procedure is applied to design an orbit controller for the *Compact Linear Collider* (CLIC). As a target function, the luminosity will be minimised. The flexibility of the design method will be demonstrated by using the available design freedom to cope with a problem arising from the specific structure of CLIC.

To evaluate the effectiveness of the ground motion optimised orbit controller, an integrated simulation framework has been set up (section 5). This simulation framework combines and extends existing codes to perform full-scale simulations that include beam tracking, realistic ground motion misalignments produced by a ground motion generator and the beam-beam interactions. Also all ground motion mitigation methods of CLIC have been implemented. Beside simulations of the luminosity performance over different time scales, also robustness studies (section 6) will be presented. A discovered sensitivity to beam energy variations will be addressed by filtering the dispersive orbit from the measurement data.

2. Modeling

The orbit controller design in this work is based on models of the beam orbit excitations in the accelerator and site-dependent ground motion models, which are briefly introduced. It will turn out in section 4 that besides the accelerator and ground motion models also a model of the ground motion induced beam offset in the BPMs is required for the controller design. Such beam oscillation models can be calculated from the accelerator and ground motion models as will also be shown in this section.

2.1. Accelerator model

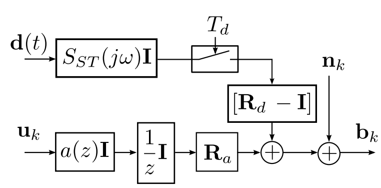

Figure 1: Block diagram of the model describing the beam oscillations along the beamline. The details are explained in the text.

In this section the accelerator system is described in a mathematical framework. As the accelerator is a discrete-time system, the so-called $\mathcal{Z}$-transform is used for its representation [13]. The $\mathcal{Z}$-transform transforms a discrete-time signal or system into its frequency representation and is therefore analogous to the Laplace-transform, used for continuous systems.

The accelerator model is depicted in Figure 1. The BPM readings $\boldsymbol{b}_k$ (where k is the discrete-time index) are influenced by

- the BPM noise $\boldsymbol{n}_k$;
- the positions of the quadrupoles via the quadrupole response matrix $\boldsymbol{R}_d$ and the positions of the BPMs themselves $(-\boldsymbol{I})$. The quadrupoles and BPMs are displaced by the continuous ground motion $\boldsymbol{d}(t)$ folded with the stabilisation transfer function $S_{ST}(j\omega)$. The element positions are sampled with a repetition time T_d;
- the actuator (corrector) settings $\boldsymbol{u}_k$ via the actuator dynamics $a(z)$ and actuator response matrix $\boldsymbol{R}_a$.

As actuators, corrector dipole magnets or mechanically movable quadrupoles can be used for example. In the latter case $\boldsymbol{R}_a$ is equal to $\boldsymbol{R}_d$. It is assumed that all actuators have the same dynamics $a(z)$ and all elements have the same stabilisation transfer function $S_{ST}(j\omega)$.

Characteristics of the accelerator system are its large size (multi-input multi-output (MIMO)) and its relatively simple structure without internal back coupling.

2.2. Ground motion models

Two types of ground motion models are used in this paper: the *ATL law* and models based on the *two-dimensional power spectral density* (PSD). Both models include correlations in time and space. For long time periods (longer than several minutes) the relatively simple ATL law is applied (see [12] for further information). However, some short time scale effects like technical noise and the micro-seismic peak (a strong ground motion in the 0.15 Hz region caused by ocean waves coupling to the shore) are not taken into account [11]. Therefore, for short time scales, models based on the two-dimensional PSD $P(\omega, k)$ are used to model the more complex high-frequency ground motion behaviour properly. The two-dimensional PSD corresponds to a superposition of independent ground motion waves with an angular frequency ω and a wave number k. Contrary to the ATL law, the short time scale models are only valid for a limited time, typically up to one minute.

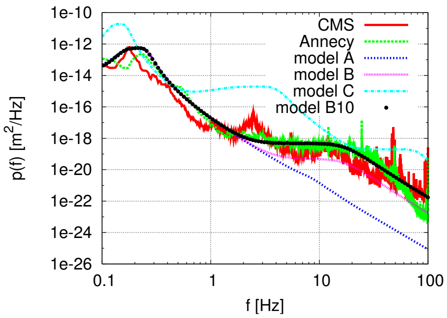

Figure 2: Ground motion power spectral density for several sites and models.

A generic form for ground motion models based on the two-dimensional PSD has been developed in [11]. The open parameters of this generic model can be adapted to the site-dependent ground motion properties. Three different scenarios taken from literature have been considered in this work (see Figure 2). Model A is based on measurements in the empty LEP tunnel, which is a very quiet site. Model B corresponds to measurements on the Fermilab site. Model B10 is model B with an amplified peak to match technical noise measured at LAPP (Annecy) [14] and in the CMS hall [15]. The according model parameters are summarised for example in [16].

2.3. Beam oscillations due to ground motion

Beam oscillations due to ground motion are mainly caused by the misalignment of the quadrupole magnets. A model for the spectra of the BPM readings due to these beam oscillations can be derived with the help of the two-dimensional ground motion PSD. Taking into account the action of the quadrupole stabilisation system $S_{ST}(j\omega)$, the spectra $B_i(\omega)$ of the BPM readings of the i^{th} BPM can be written as

$$B_i(\omega) = \frac{1}{2\pi} \int_{-\infty}^{+\infty} P(\omega, k) \left| S_{ST}(j\omega) \right|^2 G_i(k)^2 dk, \tag{1}$$

The term $G_i(k)$ describes the average beam offset in the i^{th} BPM due to a ground motion wave with wave number k and an amplitude of 1. An expression for $G_i(k)$ can be found by modifying the derivation of the spectrum of the beam-beam offset in [11] slightly, which leads to (see [16] for more details)

$$G_i(k)^2 = \sum_{m=0}^{N_i+1} \sum_{n=0}^{N_i+1} r_{i,m} r_{i,n} \cos(kL_{m,n}), \tag{2}$$

where N_i is the index of the last quadrupole influencing the i^{th} BPM and $L_{m,n}$ is the distance between the quadrupoles m and n. The parameter $r_{i,j}$ describes the change of the beam offset b_i in the i^{th} BPM due to a change of the misalignment x_j of the j^{th} quadrupole. To shorten the notation, the terms $r_{i,0}$ and r_{i,N_i+1} are used to describe the beam offset in the BPMs due to an initial beam offset and a misalignment of the BPM respectively. This leads to the definition

$$r_{i,j} = \begin{cases} 1 - \sum_{m=1}^{N_i} r_{m,j}, & \text{for } j = 0, \\ \mathrm{d}b_i/\mathrm{d}x_j, & \text{for } j = 1, 2, \ldots, N_i, \\ -1, & \text{for } j = N_i + 1. \end{cases}$$

Even though the expression for $G_i(k)$ in Eq. (2) seems to be difficult to evaluate, the spectra for all BPMs can be very efficiently calculated. By introducing the vector $\boldsymbol{G}(k)$, whose i^{th} element is $G_i(k)$, and expanding the cosine term with trigonometric identities, Eq. (2) can be rewritten as (see [16] for details)

$$\begin{gathered} \boldsymbol{G}(k)^2 = \left[\tilde{\boldsymbol{R}}_d \boldsymbol{c}(k)\right]^{\circ 2} + \left[\tilde{\boldsymbol{R}}_d \boldsymbol{s}(k)\right]^{\circ 2} \quad \text{with} \\ \tilde{\boldsymbol{R}}_d = \begin{bmatrix} \tilde{\boldsymbol{r}} & \boldsymbol{R}_d & -\boldsymbol{I} \end{bmatrix}, \quad \tilde{r}_i = r_{i,0}, \end{gathered} \tag{3}$$

where $^{\circ 2}$ symbolises the element-wise square of a vector also called Hadamard's square, $\boldsymbol{R}_d$ is the orbit response matrix due to quadrupole magnet misalignments, $\boldsymbol{I}$ is the identity matrix and

$$c_i(k) = \begin{cases} \cos(z_{i-1}k), & \text{for } i = 1, \ldots, N_q + 1, \\ \cos(\tilde{z}_{i-N_q-1}k), & \text{for } i = N_q + 2, \ldots, N_q + N_b + 1, \end{cases}$$

$$s_i(k) = \begin{cases} \sin(z_{i-1}k), & \text{for } i = 1, \ldots, N_q + 1, \\ \sin(\tilde{z}_{i-N_q-1}k), & \text{for } i = N_q + 2, \ldots, N_q + N_b + 1, \end{cases}$$

where $c_i(k)$ and $s_i(k)$ are the i^{th} element of $\boldsymbol{c}(k)$ and $\boldsymbol{s}(k)$, z_0 is the longitudinal position of the entrance of the beamline, z_i and $\tilde{z}_i$ are the longitudinal positions of the i^{th} quadrupole and BPM respectively and N_q and N_b are the total numbers of quadrupoles and BPMs in the beam line. Note that too much noise in the response matrix $\boldsymbol{R}_d$ can lead to numerical problems at the evaluation of expression Eq. (3).

3. Beam-based Orbit Controller

An orbit controller uses the BPM measurements $\boldsymbol{b}_k$ to calculate corrector settings for the next time step $\boldsymbol{u}_{k+1}$. These actuator settings are supposed to steer the beam back onto its nominal trajectory.

A semi-automatic design procedure for an high performing SVD-based orbit controller will be presented. The design procedure consists of the following three steps.

- Decoupling of inputs and outputs
- General time dependent filter design for all decoupled channels
- Gain optimisation for each decoupled channel

3.1. Decoupling

For the orbit feedback system an SVD controller is chosen, which is a special form of a decoupling controller [17]. A decoupling procedure converts a MIMO system into a new system, in which every input acts only on one output. For each of the decoupled system channels an independent single-input single-output (SISO) controller can be designed. This splitting of one large control problem into many smaller ones simplifies the design procedure significantly. For an SVD controller, the decoupling is achieved by using the SVD of the response matrix $\boldsymbol{R}_d = \boldsymbol{U}\boldsymbol{\Sigma}\boldsymbol{V}^T$, where $\boldsymbol{U}$ and $\boldsymbol{V}$ are orthonormal matrices and $\boldsymbol{\Sigma}$ is a diagonal matrix with the singular values σ_i as elements. An important property of an orthonormal matrix $\boldsymbol{A}$ is that $\boldsymbol{A}^T\boldsymbol{A} = \boldsymbol{I}$. If the system in Figure 1 is pre-multiplied with $\boldsymbol{V}$ and post-multiplied with $\boldsymbol{U}^T$, the new decoupled system

$$\begin{aligned} \hat{\boldsymbol{b}}_k &= \boldsymbol{U}^T\boldsymbol{U}\boldsymbol{\Sigma}\boldsymbol{V}^T\boldsymbol{V}\hat{\boldsymbol{u}}_{k-1} = \boldsymbol{\Sigma}\hat{\boldsymbol{u}}_{k-1}, \quad \text{with} \\ \hat{\boldsymbol{b}}_k &= \boldsymbol{U}^T\boldsymbol{b}_k \quad \text{and} \quad \hat{\boldsymbol{u}}_k = \boldsymbol{V}^T\boldsymbol{u}_k \end{aligned} \tag{4}$$

is formed. The inputs and outputs of the new system ($\hat{\boldsymbol{u}}_k$ and $\hat{\boldsymbol{b}}_k$) do not correspond to individual correctors and BPMs anymore, but to input and output vector directions, given by the columns of $\boldsymbol{U}$ and $\boldsymbol{V}$. Consequently, also the ground motion and the BPM noise have to be transformed to $\hat{\boldsymbol{d}}_k = \boldsymbol{V}^T\boldsymbol{d}_k$ and $\hat{\boldsymbol{n}}_k = \boldsymbol{U}^T\boldsymbol{n}_k$. Since the system has no internal back coupling, the decoupling is valid for all frequencies, which is usually not achievable.

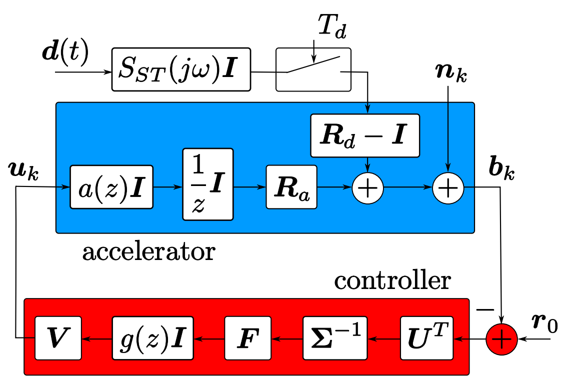

Figure 3: Block diagram of the orbit feedback system, where the values f_i and $1/\sigma_i$ have been collected in the diagonal matrices $\boldsymbol{F}$ and $\boldsymbol{\Sigma}^{-1}$

3.2. Time dependent Filter

For each of the decoupled channels an individual controller of the form $g(z)f_i/\sigma_i$ is designed, where i is the channel index. The division by the singular value σ_i corresponds to a normalisation of the loop gain in Eq. (4). The time dependent filter $g(z)$ is parametrised the same way for all controllers to reduce the problem complexity. Additionally, one gain factor f_i is left open per channel to account for the different ground motion excitations and BPM noise for each channel. The complete system is visualised in Figure 3, where $\boldsymbol{r}_0$ is the target beam orbit which is different from zero in the BDS.

The designer is free to choose the time dependent filter $g(z)$ according to his needs. The filter changes the frequency response of the open loop to achieve required results (loop-shaping method [17]). Here, we propose a time dependent filter that is composed of 4 parts:

$$g(z) = I(z)L(z)P(z)E(z).$$

Integrator $\boldsymbol{I(z)}$: The central element of $g(z)$ is the integrator

$$I(z) = \frac{z}{z-1}.$$

This element ensures good suppression of low frequency ground motion, but amplifies BPM noise strongly.

Low pass filter $\boldsymbol{L(z)}$: To improve the noise behaviour of the controller a low pass filter

$$L(z) = \frac{z(1-e^{-\frac{T_d}{T_1}})}{z-e^{-\frac{T_d}{T_1}}}$$

is added, with T_d the sampling rate and T_1 a time constant that determines the cutoff frequency, i.e. how fast the controller reacts to the measured BPM values. It is a basic first-order low pass filter multiplied by z to avoid the large phase change for high frequencies [16].

Peak element $\boldsymbol{P(z)}$: This element is added to allow the possibility to strengthen and weaken the controller performance in certain frequency ranges by adding higher gain in these ranges. This enables the user to incorporate system-specific knowledge to the design. An example will be given in section 4.

To increase the gain only in a limited frequency range, $P(z)$ is chosen as

$$P(z) = \frac{(1-n_1)(1-n_2)}{(1-z_1)(1-z_2)} \cdot \frac{(z-z_1)(z-z_2)}{(z-n_1)(z-n_2)},$$

where the poles $n_{1,2}$ and the zeros $z_{1,2}$ are conjugate complex pairs of the form $\exp((-a \pm jb)T_d)$, with $b \in \mathbb{R}$ and $a \in \mathbb{R}^+ \backslash \{0\}$ to ensure that $P(z)$ is stable and minimum-phase. The poles $n_{1,2}$ create a low-pass of second order, where the location of the poles is chosen to create a significant overshoot of the frequency response in a limited frequency range before the cutoff frequency. The zeros $z_{1,2}$ do not alter the frequency response of $P(z)$ for low frequencies, but create amplification at high frequencies, which cancels the effect of the low pass of the denominator. By positioning the poles and zeros such that the high frequency effect of the denominator and the nominator cancels completely, only the overshoot of the two second order elements remains, which creates the desired peak in the frequency response in a limited frequency range.

Phase lifting element $E(z)$: The combination of $I(z)$, $L(z)$ and $P(z)$ can lead to insufficient stability properties. An important measure for the stability of a control circuit is the phase margin, defined as the difference of the phase of the open loop frequency response at the cross-over frequency (magnitude of one) and $-180°$ (Nyquist criterion). The element

$$E(z) = \frac{1 - n_3}{1 - z_3} \cdot \frac{z - z_3}{z - n_3}$$

is added to increase the phase margin. Therefore, the zero z_3 is positioned to lift the phase shortly before the cross-over frequency. The pole n_3 is positioned to cancel the action of the zero z_3 for frequencies above cross-over frequency. Both z_3 and n_3 are located on the real axis of the z-plane inside the unit circle, which can be achieved by chosing them as $\exp(-aT_d)$ with $a \in \mathbb{R}^+\backslash\{0\}$. The phase increase and the resulting inevitable magnitude amplification can be adjusted by moving the positions of the pole and the zero .

3.3. Gain optimisation

For each controller loop there remains one gain parameter f_i, which can be chosen to minimise the power of each output signal with respect to the system excitation. The power of the output signal $\hat{b}_{i,k}$ can be calculated from the power spectra $\hat{B}_i(\omega)$, which are given by

$$\hat{B}_i(\omega) = \hat{S}_i(z = e^{j\omega T_d})\hat{D}_i(\omega) - \hat{T}_i(z = e^{j\omega T_d})\hat{N}_i(\omega),$$

where we use that the $\mathcal{Z}$-transform of a system evaluated at $z = \exp(j\omega T_d)$ corresponds to the transfer function of the system. The ground motion suppression and noise transfer functions $\hat{S}_i(z)$ and $-\hat{T}_i(z)$ of the system are given by

$$\hat{S}_i(z) = \frac{1}{1 + \hat{G}_i(z)\hat{C}_i(z)}, \quad \hat{T}_i(z) = \frac{\hat{G}_i(z)\hat{C}_i(z)}{1 + \hat{G}_i(z)\hat{C}_i(z)},$$

where $\hat{G}_i(z)$ and $\hat{C}_i(z)$ are the $\mathcal{Z}$-transforms of the decoupled system channel and its associated controller given by $\hat{G}_i(z) = a(z)\sigma_i/z$ and $\hat{C}_i(z) = g(z)f_i/\sigma_i$.

To calculate the channel ground motion spectra $\hat{D}_i(\omega)$ it is not possible to simply project the basic spectrum $D(\omega, k)$ on the channel input vectors $\boldsymbol{v}_i$. The problem with this approach is that the projection results in correlation between the individual channel spectra $\hat{D}_i(\omega)$. This correlation is not taken in consideration by the used model that assumes that all $\hat{D}_i(\omega)$ are independent of each other. This leads to large errors when the channel BPM spectra $\hat{B}_i(\omega)$ are calculated from the $\hat{D}_i(\omega)$. For that reason, virtually independent channel ground motion spectra $\hat{D}_i(\omega)$ are calculated by

$$\hat{D}_i(\omega) = s_i^{-1}\hat{B}_i(\omega), \tag{5}$$

which creates in the model the correct channel BPM spectra $\hat{B}_i(\omega)$, where s_i is the channel singular value of $\boldsymbol{R}_a$. The calculation of the channel BPM spectra $\hat{B}_i(\omega)$ is very similar to the calculation of the BPM spectra $B_i(\omega)$ as performed in section 2.3, only that $B_i(\omega)$ has to be additionally projected on the output directions $\boldsymbol{u}_i$. Hence $\hat{B}_i(\omega)$ can be calculated with Eqs. (1) and (3), only that (3) has to be slightly modified to

$$\boldsymbol{G}(k)^2 = \left[\boldsymbol{U}^T\tilde{\boldsymbol{R}}_d\boldsymbol{c}(k)\right]^{\circ 2} + \left[\boldsymbol{U}^T\tilde{\boldsymbol{R}}_d\boldsymbol{s}(k)\right]^{\circ 2}.$$

The decoupled noise spectra $\hat{N}_i(\omega)$ can be modelled as white noise (flat spectrum). Neglecting correlation, the according variances are given by the diagonal elements of the expression $\mathbb{E}\{\hat{\boldsymbol{n}}_k\hat{\boldsymbol{n}}_k^T\} = \boldsymbol{U}^T\mathbb{E}\{\boldsymbol{n}_k\boldsymbol{n}_k^T\}\boldsymbol{U}$, where $\mathbb{E}\{.\}$ is the expectation value of a random variable.

To find the optimal value for f_i, the signal $\hat{b}_{i,k}(f_i)$ is minimised with respect to the power norm. This is equivalent to minimising the L_1-norm of the power spectrum of $\hat{b}_{i,k}$

$$\min_{f_i} ||\hat{b}_{i,k}(f_i)||_{pow} = \min_{f_i} ||\hat{B}_i(\omega, f_i)||_1 = \min_{f_i} \int_{\omega=-\infty}^{+\infty} \hat{B}_i(\omega, f_i)d\omega \quad \forall i \tag{6}$$

Eq. (6) can be solved numerically by evaluating the integral for different values of f_i over a sufficient frequency range.

These parameters f_i can be optimised for different target functions than the beam orbit by modeling the influence of the ground motion onto the target function. An example of a luminosity optimised design will be shown in the adaptation to the CLIC case.

4. Adaptation to the CLIC case

In this section, after a general introduction to CLIC and its ground motion mitigation techniques, an orbit controller based on the method that was proposed in the previous section is designed for the main linac (ML) and beam delivery system (BDS).

4.1. Introduction to CLIC

CLIC [2] is an electron-positron collider, which is together with the International Linear Collider (ILC) the most promising proposal for a future high energy linear accelerator. Its main parameters are summarised in Table 1. CLIC implements a novel two-beam acceleration scheme where the main beam, which is used for the collisions, is accelerated by a second so called drive beam. The very small bunch interval Δ_b of the main beam does not allow for a global intra-train feedback in the ML and BDS, and thus the orbit controller will act from train to train with a repetition rate f_R.

The CLIC ML accelerates the beams to the final energy and is about 20 km long. It has a FODO lattice with a gradually increasing cell length to accustom to the increasing energy. The CLIC BDS [18] is mainly responsible for collimation and for the focusing of the beams to the required very small beam sizes σ_x^* and σ_y^* at the interaction point (IP).

4.2. CLIC ground motion mitigation techniques

To counter the impact of the ground motion several mitigation techniques are deployed in CLIC. Currently there are four mitigation techniques foreseen,

Centre of mass energy	E	3 TeV
Total/peak (1 %) luminosity	$\mathcal{L}/\mathcal{L}_{1\%}$	$5.9/2.0\ \times 10^{34}\,\mathrm{cm}^{-2}\,\mathrm{s}^{-1}$
Hor./vert. beam size at IP	$\sigma^*_{x/y}$	40/1 nm
Hor./vert. norm. emittance at IP	$\epsilon^*_{x/y}$	660/20 nm rad
Nr. of particles per bunch	N	$3.72\ \times 10^9$
Repetition rate	f_R	50 Hz
Nr. bunches per beam train	N_b	312
Bunch interval	Δ_b	0.5 ns
RF gradient	G_{RF}	100 MV/m

Table 1: Most important design parameters of CLIC.

namely the quadrupole stabilisation, preisolator, orbit controller and IP feedback. They will be shortly summarised.

The IP feedback [19, 20] corrects the beam-beam offset at the IP on a train to train basis by measuring the deflection angles of the colliding beams and adjusting the beam position with a dipole kicker positioned between QD0 and the IP. An additional intra-train IP feedback is foreseen to work within the bunch train. The intra-train IP feedback is considered as a reserve option and is not taken into account in this paper, contrary to the regular IP feedback.

Note that since the repetition rate of CLIC is 50 Hz, beam-based feedbacks (orbit controller and IP feedback) are mostly effective for frequencies below a few Hz. For higher frequencies other systems have to be deployed. To reduce the motion of the quadrupoles for high frequencies (≥ 1 Hz), each quadrupole will be positioned on an active stabilisation system [6]. Its theoretical transfer function is shown in Figure 4. The peak at 0.2 Hz of the quadrupole stabilisation is close to the micro-seismic peak which is unfavorable. Therefore, a targeted future design is shown in the figure as well. The final doublet, the last quadrupoles QD0 and QF1, which are especially sensitive to luminosity loss due to ground motion, will be put on a large mass block supported by air springs, the preisolator [21]. The preisolator acts as a passive ground motion isolation system. The combined

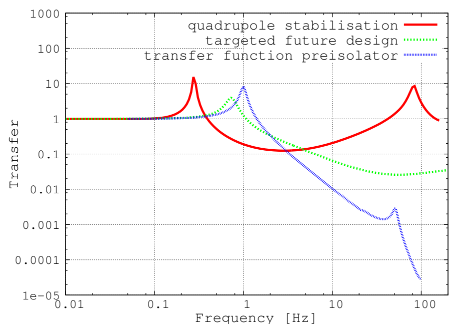

Figure 4: Amplitude of the theoretical transfer functions of the quadrupole stabilisation.

transfer function is shown in Figure 4.

4.3. Adaptation of the orbit controller

In this section, the orbit controller that was described in section 3 will be tuned to the CLIC case. The current baseline for the CLIC actuators is quadrupole movers and dipole kickers as an alternative option. For the quadrupole movers a perfect actuator response $a(z) = 1$ is assumed. This is in accordance with the specifications of the actuator design [22]. The orbit controller in the ML and BDS has 2122 BPMs and 2104 correctors to its avail.

4.3.1. Time dependent filter

The parameters chosen for the time dependent filter are as follows. For the low-pass $L(z)$, T_1 was chosen as 0.1 s. In this case the $L(z)$ demagnifies signals above its cutoff frequency of about 1.4 Hz.

As mentioned in the previous section, the final doublet quadrupoles and the other quadrupoles are stabilised by different methods (preisolator and quadrupole stabilisation). The according transfer functions differ strongly around 0.3 Hz, see Figure 4, which causes a beam offset in the final doublet quadrupoles resulting in beam size growth at the IP due to dispersion and coupling. The element $P(z)$ has been chosen to strengthen the controller in this frequency range by using $z_{1,2} = \exp((-1.43 \pm 0.4\pi j)T_d)$ and $n_{1,2} = \exp((-0.3 \pm 0.6\pi j)T_d)$.

This combination of $I(z)$, $L(z)$ and $P(z)$ leads to an insufficient phase margin. To improve the stability properties $E(z)$ with $z_3 = \exp(-17T_d)$ and $n_3 = \exp(-38T_d)$ is added to increase the phase margin to 36.3°.

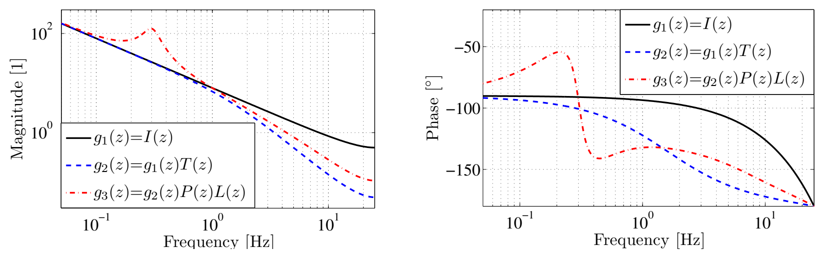

Figure 5: Magnitude (left) and phase (right) of the frequency responses of the elements of the time dependent filter $g(z)$.

The frequency responses of combinations of the elements for the time dependent filter $g(z)$ are shown in Figure 5. It can be seen that $L(z)$ reduces the sensitivity of the controller for high frequencies above the cutoff frequency, that $P(z)$ strengthens the controller in the region around 0.3 Hz and that $E(z)$ increases the phase margin, while slightly increasing the sensitivity to high frequencies.

4.3.2. Gain optimisation

By solving Eq. (6) the gain factor of each controller loop is optimised to reduce the ground motion offsets in the BPMs. However, the ultimate objective of CLIC is to reduce the luminosity loss. The equation is slightly modified to account for this objective. The luminosity loss due to ground motion is caused by two effects, beam-beam offset at the IP and beam size growth. For each controller loop i the peak luminosity loss ΔL_i, which can be decomposed in the peak luminosity loss due to beam-beam offset $\Delta L_{o,i}$ and due to beam size growth $\Delta L_{c,i}$, is estimated. This is accomplished by simulations that misalign the quadrupoles with the i^{th} column of $\boldsymbol{V}$ and calculate ΔL_i and $\Delta L_{c,i}$ by centering the beams. For small values $\Delta L_{o,i}$ can be calculated with $\Delta L_{o,i} = \Delta L_i$ -$\Delta L_{c,i}$. The normalised peak luminosity losses for the vertical direction are shown in Figure 6.

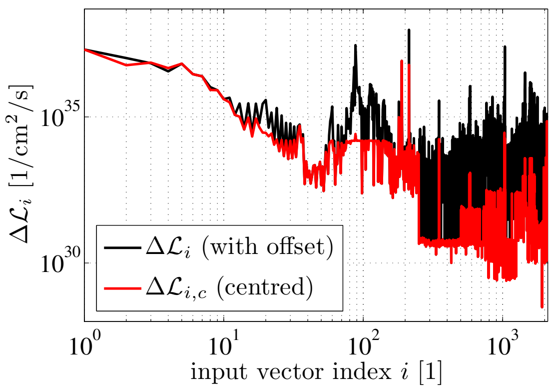

Figure 6: Normalised peak luminosity loss due to beam-beam offset at the IP and beam size growth (centred) for each decoupled controller loop for the vertical direction.

The modified version of Eq. (6) becomes:

$$\min_{f_i} \int_{\omega=-\infty}^{+\infty} \hat{B}_i(\omega, f_i) \left(\frac{\Delta L_{c,i}}{\Delta L_i} + \frac{\Delta L_{o,i}}{\Delta L_i} \left| \frac{1}{z} S_{IP}(e^{j\omega T_d}) \right|^2 \right) d\omega, \tag{7}$$

where $1/zS_{IP}(\exp(j\omega T_d))$ is the frequency response of the IP feedback, which has to be taken into account. The gain factors obtained with this method for ground motion model B10 are shown in Figure 7 for both the horizontal and vertical direction. It can be seen that all 2104 gain factors are below 1 and have been artificially given a minimum value of 10^{-6} to avoid any open control loops.

5. Simulations

5.1. Simulation framework

All simulations are performed tracking the beams through both MLs and BDSs of CLIC with PLACET [23] and beam-beam interaction code GUINEA-PIG [24], similar as in [25] for the ILC. A BPM resolution of 100 nm is assumed for the ML BPMs and 50 nm for the BDS BPMs. A ground motion generator that simulates the short term and long term ground motion models of section

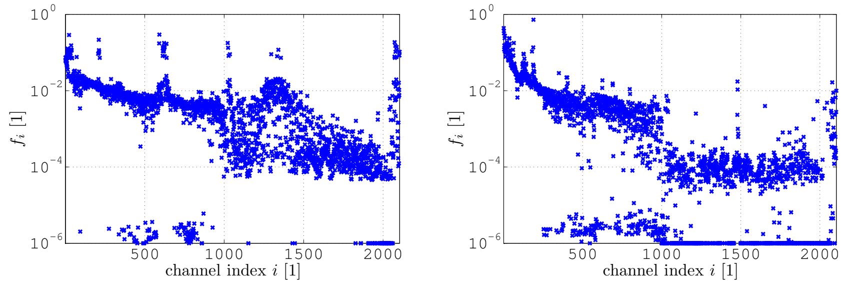

Figure 7: Gain factors f_i of the decoupled control loops for the horizontal (left) and vertical (right) direction.

2.2, all ground motion mitigation methods of section 4.2 and the controller of section 4.3 have been integrated in the simulations. Both the current version and the future design of the quadrupole stabilisation are studied. Besides the automatically tuned controller gains of Figure 7, a former hand-tuned version of the controller gains is tested for comparison.

5.2. Pre-assumptions

The foreseen emittance budget due to the static imperfections of the RTML, ML and BDS combined is a growth from 5 nm rad normalised geometric emittance at the exit of the damping rings to 20 nm rad at the IP. Instead of integrating the static imperfections directly in the simulations, a simplified approach is taken by injecting a beam with an emittance of 20 nm rad at the beginning of the ML (instead of 10 nm rad) to approximate the static imperfections budget. This approach makes the assumption that the effects of the static and dynamic imperfections can be factorised and that the misaligned lattice is not adversely effecting the orbit feedback operation. Further studies will be carried out to understand the combined effect. The foreseen budget for peak luminosity loss due to dynamic imperfections in the ML and BDS is about 20%.

5.3. Luminosity evolution for short time scales

The short term ground motion generator based on the two-dimensional PSD $P(\omega, k)$ misaligns the beamline every pulse. All of the four mitigation techniques are applied, i.e. preisolator, quadrupole stabilisation, IP feedback and orbit controller. Figure 8 shows that the luminosity is well preserved over a time period of 60 s, which is about the maximum time for which the used ground motion generator is valid.

The jitter on the luminosity is caused by the remaining high frequencies of the ground motion and the BPM noise.

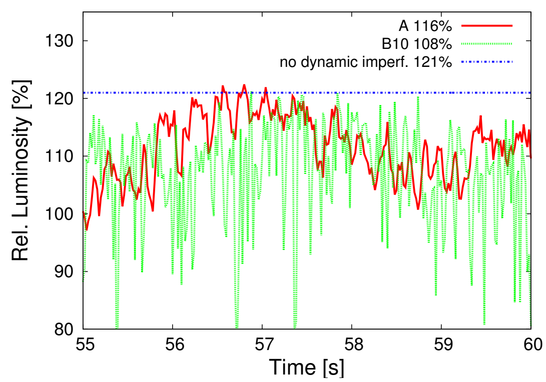

Figure 8: Example of peak luminosity for the current design over a longer time scale (60 s) for several ground motion models.

In Table 2 the relative peak luminosity performance using the auto-tuned controller for several configurations of the applied stabilisation system and the ground motion model are shown. Note that for each result a different controller has been used, since the f_i were optimised with respect to the stabilisation system and the ground motion model according to Eq. (7). It can be concluded that depending on the ground motion different stabilisation measures are required. Note that for ground motion model A mitigation methods can even lower the luminosity performance. This is due to offsets between the preisolator and the rest of the beamline, which is caused by a discrepancy between the two transfer functions. Also note that an enhanced quadrupole stabilisation can improve the luminosity performance significantly.

The auto-tuned controller (named C_5) is compared in the following with other global feedback algorithms. The controller C_1 is considered to be the

Stabilisation	no GM	A	B	B10
Current	121 (0)	117 (4)	116 (5)	109 (12)
Future	121 (0)	121 (0)	121 (0.5)	120 (1)

Table 2: Overview of the peak luminosity performance (and luminosity loss) in % with respect to the nominal peak luminosity $\mathcal{L}_{1\%}$ for different ground motion (GM) models and quadrupole stabilisation system averaged over 20 seeds.

standard SVD feedback that employs an integrator instead of $g(z)$ and a basic weighting of the modes by using $\hat{f}_i = 1$, $\forall i \leq 20$ and $\hat{f}_i = 10^{-4}$, $\forall i > 20$. The next two controllers improve the basic controller C_1 by using either the optimised gains f_i of C_5 (C_2) or the optimised time dependent filter $g(z)$ instead of the integrator (C_3). Finally, C_4 consists of the optimised time dependent filter $g(z)$ and gains $\tilde{f}_i$ that have been optimised by hand by applying the knowledge of Figure 6.

GM model	C_1	C_2	C_3	C_4	C_5
B	24 (97)	103 (18)	24 (97)	111 (10)	116 (5)
B10	23 (98)	97 (24)	23 (98)	107 (14)	109 (12)

Table 3: Peak luminosity performance (and luminosity loss) in % with respect to the nominal peak luminosity $\mathcal{L}_{1\%}$ of different controllers (C_1 to C_5) for different ground motion models B and B10. The current stabilisation system was used and the results are averaged over 10 seeds.

As can be seen in Table 3, the application of non-optimised gains f_i results in a very large luminosity loss (controllers C_1 and C_3). Also the use of optimised gains without optimising the time dependent filter (controller C_2) causes still too strong performance degradation. Only the controllers C_4 and C_5 can preserve the luminosity to an acceptable level. The reason is that for the design of both controllers detailed system model information has been used. It should also be pointed out that C_5 still performs better than C_4 even though the gains f_i for C_5 have been found automated within a few minutes of calculation, while for

C_4 several weeks of hand tuning has been necessary.

5.4. Luminosity evolution for large time scales

For longer time scales the ground motion generator based on the two-dimensional PSDs is no longer valid. In addition, the simulations would become computationally intensive. Therefore, to study ground motion for longer time scales the ATL law has been applied with the constant $A = 0.5 \cdot 10^{-6}\,\mu\mathrm{m}^2/(\mathrm{s\,m})$, which is based on measurements from the LEP-tunnel. After applying the orbit controller the resulting relative peak luminosity for CLIC is shown in Figure 9 as a function of time. It can be seen that after about half an hour the peak luminosity is decreased by 10% and further optimisation is required. However, it has been shown that tuning the accelerator with the BDS sextupole knobs [5] can recover the luminosity fully. Since these BDS sextupole knobs are not deployed in the orbit controller, this shows that the response matrix of the accelerator does not change significantly for this time scale and therefore the orbit controller performs well. Further studies will have to be done to estimate the time period for which the response matrix is still accurate.

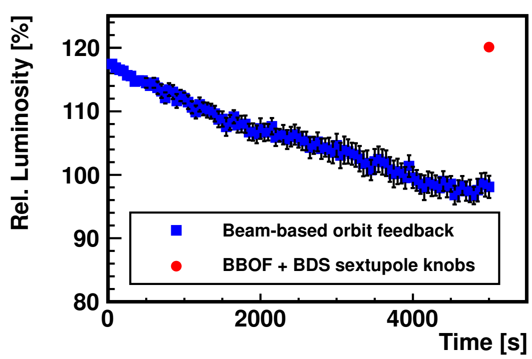

Figure 9: Peak luminosity evolution for long time scales of ground motion. After about 30 minutes, the luminosity is decreased by 10%. To correct for this loss, further optimization procedures, e.g. tuning of the BDS sextupole knobs, are required.

6. Robustness Studies

The robustness of the CLIC orbit controller has been studied in detail. Many types of dynamic and static imperfections and their effect on the controller performance have been studied and the controller has been found to be sufficiently robust for all tested imperfections. If not stated differently, the studies were carried out with the auto-tuned controller optimised for ground motion B10 and the current stabilisation function. Two types of imperfections (BPM resolution and beam energy jitter) are especially important for the CLIC controller and are therefore discussed separately. The outcomes of the studies of the other tested imperfections are summarised in the last section and we would also like to refer also to the more detailed publications [26] and [16].

6.1. BPM resolution

BPM noise degrades the effectiveness of the orbit controller, since a BPM measurement error will propagate into the orbit correction. To evaluate the required BPM resolution in the BDS, simulations have been performed where all other dynamic effects as e.g. ground motion are not applied. In Figure 10 (left) the relative peak luminosity loss is shown as a function of the BPM resolution. It can be seen that a BPM resolution of 50 nm is required in the BDS to limit the luminosity loss to 2%, while the BPM resolution in the ML can be more relaxed. Previousy, a BPM resolution of 10 nm was considered to be necessary. However, due to consideration of static imperfections in the final focus system, tighter BPM resolutions might still be required. Also shown in Figure 10 (right) is the peak luminosity loss for different versions of the orbit controller, once with the full controller and two times with a simple integrator ($g(z) = I(z)$), with full gains ($\boldsymbol{F} = \boldsymbol{I}$) and optimised gains ($\boldsymbol{F} = \mathrm{diag}(f_i)$) respectively. It can be seen that the gain optimisation as well as the design of the low pass of the time dependent filter reduces the back-coupling of the BPM noise.

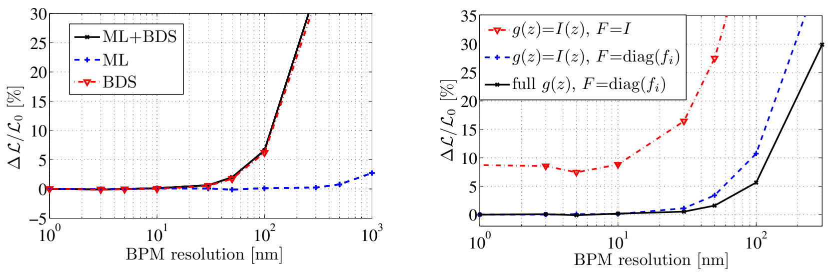

Figure 10: Relative peak luminosity loss as a function of the BPM resolution for the ML and BDS, separated and combined (left) and for different versions of the controller (right). Note that the luminosity loss is only due to BPM noise and that no other dynamic effects, e.g. ground motion, has been applied.

6.2. Beam energy jitter

The basic feedback algorithm encounters problems in the presence of beam energy jitter. This beam energy jitter is caused by small deviations of the initial beam energy and acceleration gradients from their nominal values. In the dispersive collimation section of the BDS, such energy variations result in beam offsets up to the millimetre range. The orbit controller reacts strongly on these large offsets. As a result the beam is mis-steered and the according luminosity loss is not tolerable. To counteract this effect, we deploy the fact that the beam offsets due to energy variations follow a specific pattern $\boldsymbol{b}_D$. By filtering this dispersion pattern from the BPM measurements with

$$\tilde{\boldsymbol{b}}_k = \boldsymbol{b}_k - \frac{\boldsymbol{b}_k^T \boldsymbol{b}_D}{\boldsymbol{b}_D^T \boldsymbol{b}_D} \boldsymbol{b}_D$$

the luminosity can be recovered almost fully. The use of this dispersion filtering is only necessary in the horizontal plane, since the coupling to the vertical plane can be neglected. The remaining luminosity loss due to the energy jitter coupling with the orbit controller has been observed to be 0.1%.

6.3. Other imperfections

Apart from the already mentioned imperfections, several other effects have been investigated. The scaling errors of BPMs and correctors are restricted by the orbit controller action. For a relative luminosity loss of 0.5% one can allow for a corrector scaling error up to 30%, while the BPM scaling error tolerance for the same luminosity loss is as small as 1%. The tolerances for static and jitter-like quadrupole strength errors are known to be very tight due to the lattice design. The action of the orbit controller does not worsen these tolerances in a notable way. Also the tolerances for the incoming beam jitter at the entrance of the ML are hardly altered by the orbit controller operation. Breakdown studies of BPMs, correctors and the stabilisation systems revealed sensitivity to malfunctions of certain stabilisation systems and BPMs in the BDS. An especially robust design for these systems is advisable and possibly also redundancy has to be foreseen. For the positioning capability of the stabilisation system, a tolerance of 0.25 nm has been identified. This tight tolerance has been confirmed to be achievable by the CLIC stabilisation group. In case this tolerance will turn out to be problematic for other accelerator designs, dipole kickers can be used instead of the quadrupole movers. As mentioned before, a fast and perfect actuator response $a(z) = 1$ has been assumed. For the case of CLIC, this assumption is valid as shown by the stabilisation group [22]. However, if slower actuators are used no performance degradation is expected, since the corresponding low pass behaviour of $a(z)$ can substitute parts of the artificially introduced low pass $L(z)$.

7. Conclusions

In this paper, we have presented a ground motion optimised orbit controller design method. This design method exploits a model of the beam oscillations spectra in the BPMs, which have been derived from an accelerator model, existing noise and ground motion models. The orbit controller design method consists of the three steps: decoupling of the inputs and outputs, time dependent filter design and gain optimisation. This design method was applied to create an orbit controller for CLIC. The orbit controller design method has several advantages:

- Since the design is based on SVD decoupling, the overall controller system is split up in SISO systems, which simplifies the design.
- The time dependent filter enables the user to incorporate expert knowledge.
- The tedious task of optimising each decoupled loop (several thousand in the case of the future linear accelerator) by hand is overtaken by an automated procedure. This eases the task of the designer.
- The controller design makes it possible to incorporate models of the ground motion and the measurement noise. This closes a gap between the ground motion research of the accelerator community and the orbit controller design practice in a quantitive way.
- The controller performs better than a hand tuned controller in the case of CLIC.

To evaluate the luminosity preservation ability of this controller, an integrated simulation framework was set up. Full-scale simulations revealed that the orbit controller, in combination with the other ground motion mitigation methods, is capable of keeping the ground motion induced luminosity loss within the allowed specifications. This is an essential contribution to resolve the feasibility issue of ground motion for CLIC. Furthermore, robustness studies showed that the controller is robust against imperfections, especially to measurement noise. For CLIC the required BPM resolution could be loosened from 10 nm to 50 nm in the BDS. A sensitivity to variations of the beam energy was observed, which could be resolved by filtering the resulting large dispersive orbits from the BPM measurements.

Even though the presented orbit controller design method was developed for the high demands of the future linear collider with respect to orbit stability, the generic design procedure can be easily adapted to other linear machines. To use the procedure for ring accelerators, the ground motion models would have to be extended to the circular geometry, which could be an interesting subject for future work. Alternatively, for existing accelerators the necessary power spectral densities of the BPM readings can be obtained from measurements.

References

[1] *International Linear Collider Reference Design Report, Volume 3: Accelerator*, 2007.

[2] *CLIC Parameter Table*, `http://clic-meeting.web.cern.ch/clic-meeting/clictable2010.html`

[3] K. Kubo, Phys. Rev. ST Accel. Beams 14, 014401 (2011).

[4] T. O. Raubenheimer and P. Tenenbaum, Report No. SLAC-TN-03-071, 2004.

[5] B. Dalena et al., Phys. Rev. ST Accel. Beams 15, 051006 (2012).

[6] C. Collette et al., Nucl. Instrum. Meth. A 621, (2010) 71-78.

[7] T. Himel et al., SLAC-PUB-6125, 1993.

[8] L. Hendrickson et al., In Proc. of PAC99, 1999.

[9] R. J. Steinhagen, PhD thesis, Technische Hochschule Aachen, 2007.

[10] J. Rowland, In Proc. of ICALEP07, 2007.

[11] A. Sery and O. Napoly, Phys. Rev. E 53, 5323 (1996).

[12] V. Shiltsev, Phys. Rev. Lett. 23, 238501 (2010).

[13] A. V. Oppenheimer, R. W. Schafer and J. R. Buck, *Discrete time signal processing* Prentice Hall, 1999.

[14] B. Bolzon, PhD thesis, Université de Savoie, 2007.

[15] A. Kuzmin, Report No. EDMS-1027459, CERN, 2009.

[16] J. Pfingstner, PhD thesis, to be published, 2012.

[17] S. Skogestad and I. Postlethwaite, *Multivariable Feedback Control: Analysis and Design*, Wiley-Interscience, 2005.

[18] R. Tomas et al., Report No. EUROTEV-REPORT-2008-039, 2008.

[19] J.Resta-Lopez et al., JINST 5, 9007 (2010).

[20] G. Balik et al., In Proc. of IPAC11, 2011.

[21] A. Gaddi et al., `https://edms.cern.ch/file/1098581/3/LCD-2010-011.pdf`

[22] K. Artoos et al., In Proc. of IPAC12, 2012

[23] A. Latina et al., In Proc. of EPAC08, 2008.

[24] D. Schulte, In Proc. of ICAP98, 1998.

[25] G. White, N. Walker and D. Schulte, In Proc. of PAC05, 2005.

[26] J. Pfingstner et al., In Proc. of IPAC12, 2012